Bulletin of the Seismological Society of America, Vol. 98, No. 6, pp. 2746–2755, December 2008, doi: 10.1785/0120080111

Finite-Fault Analysis of the 2004 Parkfield, California, Earthquake Using P_{nl} Waveforms

by C. Mendoza and S. Hartzell

Abstract We apply a kinematic finite-fault inversion scheme to P_{nl} displacement waveforms recorded at 14 regional stations ($\Delta < 2°$) to recover the distribution of coseismic slip for the 2004 Parkfield earthquake using both synthetic Green's functions (SGFs) calculated for one-dimensional (1D) crustal-velocity models and empirical Green's functions (EGFs) based on the recordings of a single M_w 5.0 aftershock. Slip is modeled on a rectangular fault subdivided into 2×2 km subfaults assuming a constant rupture velocity and a 0.5 sec rise time. A passband filter of 0.1–0.5 Hz is applied to both data and subfault responses prior to waveform inversion. The SGF inversions are performed such that the final seismic moment is consistent with the known magnitude (M_w 6.0) of the earthquake. For these runs, it is difficult to reproduce the entire P_{nl} waveform due to inaccuracies in the assumed crustal structure. Also, the misfit between observed and predicted vertical waveforms is similar in character for different rupture velocities, indicating that neither the rupture velocity nor the exact position of slip sources along the fault can be uniquely identified. The pattern of coseismic slip, however, compares well with independent source models derived using other data types, indicating that the SGF inversion procedure provides a general first-order estimate of the 2004 Parkfield rupture using the vertical P_{nl} records. The best-constrained slip model is obtained using the single-aftershock EGF approach. In this case, the waveforms are very well reproduced for both vertical and horizontal components, suggesting that the method provides a powerful tool for estimating the distribution of coseismic slip using the regional P_{nl} waveforms. The inferred slip model shows a localized patch of high slip (55 cm peak) near the hypocenter and a larger slip area (~50 cm peak) extending between 6 and 20 km to the northwest.

Introduction

The M_w 6.0 Parkfield, California, earthquake of 28 September 2004 is one of the most widely recorded seismic events in the instrumental history of seismology due principally to monitoring efforts related to the Parkfield Earthquake Prediction Experiment (Bakun and Lindh, 1985). This experiment was designed to investigate the physical process leading up to an anticipated earthquake and resulted in increased instrumentation in the Parkfield region that included broadband and strong-motion seismic stations, local strainmeters and creepmeters, and Global Positioning System (GPS) instruments (Roeloffs and Langbein, 1994; Bakun *et al.*, 2005). Data from these sites have been previously used both individually and in combination to derive coseismic slip distributions for the 2004 Parkfield earthquake, which generally show slip extending northwest from the hypocenter for a distance of about 25–30 km (e.g., Custodio *et al.*, 2005; Langbein *et al.*, 2005; Langbein *et al.* 2006; Liu *et al.*, 2006; Hartzell *et al.*, 2007). A joint inversion of GPS and Interferometric Synthetic Aperture Radar (InSAR) data yields a similar result (Johanson *et al.*, 2006).

Langbein *et al.* (2005) compared three preliminary slip models derived using a combination of different data types and found a general similarity in the location of significant slip along the fault. Model 1 was based on static GPS and strain meter data; Model 2 was obtained using static GPS data and seismic waveforms from eight regional broadband stations located within 300 km of Parkfield; Model 3 used two regional broadband stations and one local strong-motion station in addition to static and 1 Hz GPS data. The similarity in the source models suggests that regional seismic waveforms provide some constraints on the details of the earthquake rupture process. Langbein *et al.* (2005) do not provide details on the frequency content of the seismic waveforms used to derive Models 2 and 3, but generally, studies of this type consider the entire regional wave train filtered over a broad frequency band that includes periods between 1 and 50 sec (e.g., Kaverina *et al.*, 2002). In this study, we invert the *P*-wave portion of the seismic waveforms recorded within 2° of the Parkfield earthquake to explore their use in the derivation of the earthquake rupture history. As discussed later, filtering these regional waveforms at various passbands shows coherent pulses that appear to contain information on the extended properties of the source.

P-wave energy observed at regional distances is generally complicated by the arrival of energy critically refracted from the Moho (P_n) and from the lower crust (P^*). These phases are observed beyond critical distances that depend on the thickness and velocities of the crustal layers and on the upper-mantle velocity. For example, for a 27 km thick crust with a *P*-wave velocity of 5.7 km/sec and a mantle velocity of 8.0 km/sec, P_n is observed at distances beyond about 0.5° (55 km), arriving after direct *P*. However, at epicentral distances greater than about 1.2° (130 km), P_n arrives prior to direct *P*. Long-period *PL* waves also contribute to the *P*-wave coda prior to the *SV* arrival. This collective *P*-wave energy observed at regional distances is generally referred to as P_{nl} and has been used previously to model the earthquake source mechanism (e.g., Helmberger and Engen, 1980; Wallace *et al.*, 1981).

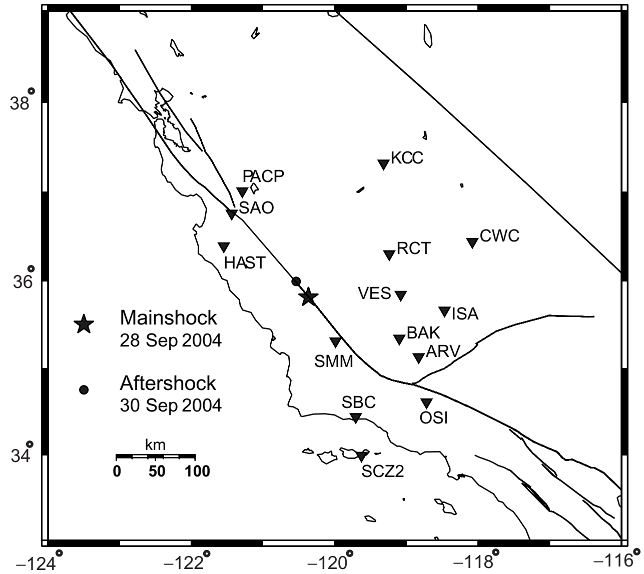

Figure 1. Regional broadband stations (triangles) that recorded the 2004 Parkfield earthquake (star) at distances less than 2° from the epicenter (35.82° N, 120.37° W). The filled circle indicates the epicentral location (35.99° N, 120.54° W) of an M_w 5.0 aftershock that occurred on 30 September 2004. Solid lines show the main strands of the San Andreas Fault system.

Data and Methodology

The 2004 Parkfield earthquake was recorded by more than 40 regional broadband seismograph stations distributed throughout central and southern California. We collected seismic waveforms from the Incorporated Research Institutions for Seismology (IRIS) database for stations located within 2° of the epicenter (Fig. 1) and removed the instrument response to obtain P_{nl} displacements (see Data and Resources section). Table 1 gives the distance and azimuth to each of the recording sites.

We applied the kinematic finite-fault inversion procedure of Hartzell and Heaton (1983) to the P_{nl} records to derive the rupture history of the earthquake. The method requires a fault plane with known geometry and prescribed dimensions to identify the coseismic distribution of slip. We used a near-vertical northwest–southeast strike-slip fault (N140°E strike, 89° dip, 180° rake), consistent with the orientation of the planar structure suggested by Thurber *et al.* (2006) based on earthquake locations and mechanisms in the Parkfield region. The fault length and width are 38 km and 12 km, respectively, with the hypocenter placed 30 km from the northwest edge of the fault at a depth of 8 km. The fault plane covers depths from 2 to 14 km and is subdivided into 114 2×2 km subfaults. Synthetic waveforms are computed for each subfault by summing the responses (Green's functions) of individual point sources distributed along the length and width assuming a constant propagation of rupture from the hypocenter and a fixed rise time of 0.5 sec.

The inversion is conducted by solving the linear system

$$\begin{bmatrix} \mathbf{A} \\ \lambda_1 \mathbf{S} \\ \lambda_2 \mathbf{M} \end{bmatrix} \mathbf{x} = \begin{bmatrix} \mathbf{b} \\ 0 \\ 0 \end{bmatrix},$$

where **A** is a matrix of the subfault synthetics for all stations, **b** is a vector containing the observed waveforms, and **x** is the solution vector that contains the amount of slip required in

Table 1
Regional Broadband Stations Located at Epicentral Distances $\Delta < 2°$ of the 2004 Parkfield Earthquake

Station	Δ (°)	AZ (°)	*T* (sec)
SMM	0.59	149	7.8
RCT	1.03	62	12.9
VES	1.04	88	12.9
HAST	1.12	301	14.5
BAK	1.13	114	14.5
SAO	1.29	318	17.5
PACP	1.40	328	18.8
ARV	1.43	118	18.8
SBC	1.47	159	20.2
ISA	1.54	95	20.2
KCC	1.72	29	22.8
OSI	1.80	131	23.9
SCZ2	1.92	162	25.0
CWC	1.95	71	25.0

AZ represents the source-to-station azimuth; *T* is the estimated duration of the P_{nl} record calculated from the Jeffreys and Bullen (1940) transmission times of near-earthquake phases.

each subfault to reproduce the observations using a least-squares minimization norm. **S** and **M** are linear constraints appended to the synthetics matrix to stabilize the inversion. These constraints are imposed by manually increasing λ_1 and λ_2 until the simplest possible solution is identified that still reproduces the observed waveforms. **S** is constructed so that the difference in slip for adjacent subfaults is zero, thus requiring a smooth transition of elements in the solution vector **x**. **M** sets the length of the **x** vector to zero, effectively reducing the seismic moment of the earthquake. In solving for **x**, a positivity constraint is additionally used to prevent back-slip on the fault.

A layered crustal structure based on the default northern California velocity model (e.g., Oppenheimer *et al.*, 1993) is initially used to compute point-source Green's functions using the frequency-wavenumber method of Zhu and Rivera (2002). This crustal structure is currently employed by the U.S. Geological Survey (USGS) Northern California Seismic Network (NCSN) to locate earthquakes in areas where a local velocity model is not available. One of our goals is to examine if this general crustal structure allows a reasonable determination of the coseismic slip pattern on the fault using the vertical P_{nl} waveforms. We also consider a more detailed 1D velocity model interpreted from the 3D crustal structure derived by Thurber *et al.* (2006) and used by Hartzell *et al.* (2007) for the northeast side of the fault in their analysis of the local strong-motion data recorded for the 2004 Parkfield earthquake. Both velocity models are given in Table 2.

Hartzell *et al.* (2007) used the same finite-fault inversion scheme in their source analysis and give a more detailed discussion of the method. The principal difference between our application and that of Hartzell *et al.* (2007) is that we use a single triangular source time function (0.5 sec) to model the propagating rupture instead of allowing multiple time windows (five) of shorter duration (0.2 sec). The use of multiple time windows allows for variations in rupture velocity along the fault, if required by the data, providing flexibility on the location of fault slip. However, inversions of the strong-motion records using a fixed 0.2 sec triangle yield results that are not very different than those obtained using multiple time windows that allow up to 1.2 sec for the fault rise time (Hartzell *et al.*, 2007). We thus fix the rise time at 0.5 sec to simplify the inversion process and use different constant rupture velocities (2.4, 2.7, and 3.0 km/sec) to examine their effect on the inferred slip model. Also, in our analysis, we adjust the moment-minimization constraint (λ_2) to identify the solution that yields a seismic moment equivalent to the known size of the earthquake (M_w 6.0). This prevents the mapping of unnecessary slip onto the source.

A record length that includes 20 sec beyond the first P arrival is used in the inversion. This time interval generally includes the P_{nl} portion of the record except for sites closer than about 1.2°, where the window also includes several seconds of later-arriving S and surface-wave energy (see Table 1). We tried using variable record lengths based on the expected duration of the P_{nl} records from Table 1, but the inversions did not yield results very different than those obtained using a fixed 20 sec time interval. A timestep of 0.1 sec is used in the inversion, with observed and synthetic waveforms aligned at the P-wave onsets. For the synthetics, these onsets correspond to the first arrivals observed on the waveforms computed for the subfault containing the earthquake hypocenter. However, small iterative adjustments in timing are also made to improve the fit between observed and synthetic records.

Table 2
Crustal-Velocity Models Used to Compute Synthetic Green's Functions for the Parkfield Earthquake

Thickness (km)	V_P (km/sec)	V_S (km/sec)	Density (g/cm^3)	Q_P	Q_S
		Model NC			
3.5	3.6	2.0	2.3	500	250
19.5	5.7	3.2	2.7	1000	500
4.0	6.8	3.8	2.9	1500	750
—	8.0	4.5	3.3	2000	1000
		Model NF			
1.0	2.0	1.1	2.0	200	100
1.0	3.5	2.0	2.3	600	300
3.0	4.5	2.6	2.3	780	390
5.0	5.4	3.1	2.7	930	465
3.0	6.5	3.8	2.8	1140	575
13.0	7.0	4.0	2.8	1200	600
—	8.0	4.5	3.4	1350	675

Model NC is based on the default gradient velocity model used by the Northern California Seismic Network to locate earthquakes in areas where a local velocity model is not available (Oppenheimer *et al.*, 1993). Model NF corresponds to the velocity structure used by Hartzell *et al.* (2007) to model near-field strong-motion records in the Parkfield region northeast of the San Andreas Fault. V and Q indicate velocities and quality factors for P and S waves.

Source Analysis

We initially conducted the inversion using synthetic Green's functions (SGFs) computed with the default northern California (NC) crustal structure given in Table 2. Generally, higher frequencies are needed to recover greater source detail, and we investigated the use of several different filters. These were applied to both data records and to subfault synthetics prior to waveform inversion. Frequency bands that allowed energy at frequencies greater than 1 Hz yielded complex data records that appeared incoherent. We therefore tried using a 0.2–1.0 Hz passband to coincide with the frequency range used to invert the near-source strong-motion data (e.g., Custodio *et al.*, 2005; Liu *et al.*, 2006; Hartzell *et al.*, 2007). However, we found that it was difficult to reproduce the first 3–5 sec of the records at many of the stations, possibly due to unmodeled receiver site effects or crustal-structure variations. This misfit to the initial portion of the record was generally improved by using a longer period band-pass filter with corners at 0.1 and 0.5 Hz.

We also tried filtering the P_{nl} records over a broad frequency band from 0.02 to 1.0 Hz and obtained results similar to those obtained using a passband of 0.1–0.5 Hz. This result indicates that high frequencies (above 0.5 Hz) in the broadband filtering play a less dominant role, making this passband equally usable in the analysis of P_{nl} records. For larger sources, with longer period slip, the passband of 0.02 to 1.0 Hz may be more appropriate. However, for the relatively small source and short rise times of the Parkfield earthquake, the inversion results are similar for the two passbands. We also tried inverting the entire wave train (70 sec) observed at the regional stations filtered between 0.02 and 1.0 Hz but were unable to fit the complexity in the waveforms, which are dominated by surface-wave energy. This may explain why other data types were used in conjunction with the regional broadband records to derive the source models presented by Langbein *et al.* (2005) for the Parkfield earthquake.

Figure 2 shows the waveform fits obtained for rupture velocities of 2.4, 2.7, and 3.0 km/sec using a 0.1–0.5 Hz passband. The initial amplitude level is generally reproduced at most of the stations, but the observed records are not fit over their entire length for any of the runs. For most of the stations, this length corresponds primarily to the P_{nl} portion of the record, as indicated earlier. However, in some cases (e.g., stations HAST, RCT, VES, BAK, SMM), the interval includes between 5 and 12 sec of *S*- and surface-wave energy at the end of the record that are also being fit in the inversion process. The lowest Euclidean Norm ($\|\mathbf{b} - \mathbf{Ax}\|$) of the residuals (Table 3) is obtained for a rupture velocity of 2.7 km/sec; however, the similar overall character of the fits between observed and predicted waveforms indicates a weak dependence of the inversion results on the rupture speed and makes it difficult to choose a single best-fit rupture velocity.

Figure 3 shows the slip models obtained for the three rupture velocities. The primary effect due to an increase in rupture speed is the general expansion of the distance range affected by the source to accommodate a rupture time of about 10 sec. The source models show slip distributed northwest of the hypocenter with slip concentrations located at different positions along the strike in response to the varying rupture velocity. These results indicate that the data are capable of identifying the general pattern of coseismic fault slip if a reasonable estimate of the rupture velocity is used. The precise location of the slip regions, however, requires a more accurate knowledge of the rupture speed.

We also performed the inversion using subfault synthetics based on the near-fault (NF) velocity structure from Table 2 assuming a constant rupture speed of 3.0 km/sec. Apart from the smoother transition in body-wave velocities offered by the additional layers, the NF model contains higher crustal velocities at depths greater than 7 km compared to the default NC structure. Also, it has lower body-wave velocities near the surface and a slightly thinner crust. The results of the inversion are shown in Figure 4. The resulting slip model shows a large region of northwest slip that is located much closer to the hypocenter compared to the results shown in Figure 3. The Euclidean Norm obtained for the inversion (Table 3) indicates that the NF crustal model provides a better numerical fit to the observed waveforms compared to the default structure. The waveforms, however, are again not completely reproduced over their entire length, and the inversion results cannot be used to designate a single representative crustal structure for all propagation paths. The results also show that reasonable modifications to the assumed crustal structure can significantly affect the imaging of the source.

In general, we were unable to reproduce the entire P_{nl} waveform at all of the stations using synthetic waveforms computed for either the NC or the NF flat-layered crustal-velocity model. Thus, we explored the use of empirical Green's functions (EGFs) in the inversion process. For this task, we examined the Northern California Earthquake Data Center catalog and the IRIS waveform database (see Data and Resources section) to identify aftershocks that were clearly recorded by most of the stations that recorded the mainshock. We found two events meeting these criteria with source mechanisms similar to that of the mainshock: an M_w 4.0 event on 28 September 2004 (origin time 19:31:28 UTC [coordinated universal time]) and an M_w 5.0 event on 30 September 2004 (origin time 18:54:29 UTC). Source mechanisms computed by Langbein *et al.* (2005) for both of these aftershocks indicate strike-slip faulting similar to that of the Parkfield earthquake. We used the larger of the two events in an EGF inversion of the P_{nl} data set. This aftershock occurred about 25 km northwest of the mainshock epicenter (see Fig. 1) at a depth of 10.5 km. Of the 14 stations listed in Table 1, only SAO did not record the event. We used the deconvolved displacement records at these 13 stations as EGFs to compute subfault responses as before with scaled, time-lagged, and summed aftershock records to simulate a rupture propagating at a constant velocity of 3.0 km/sec,

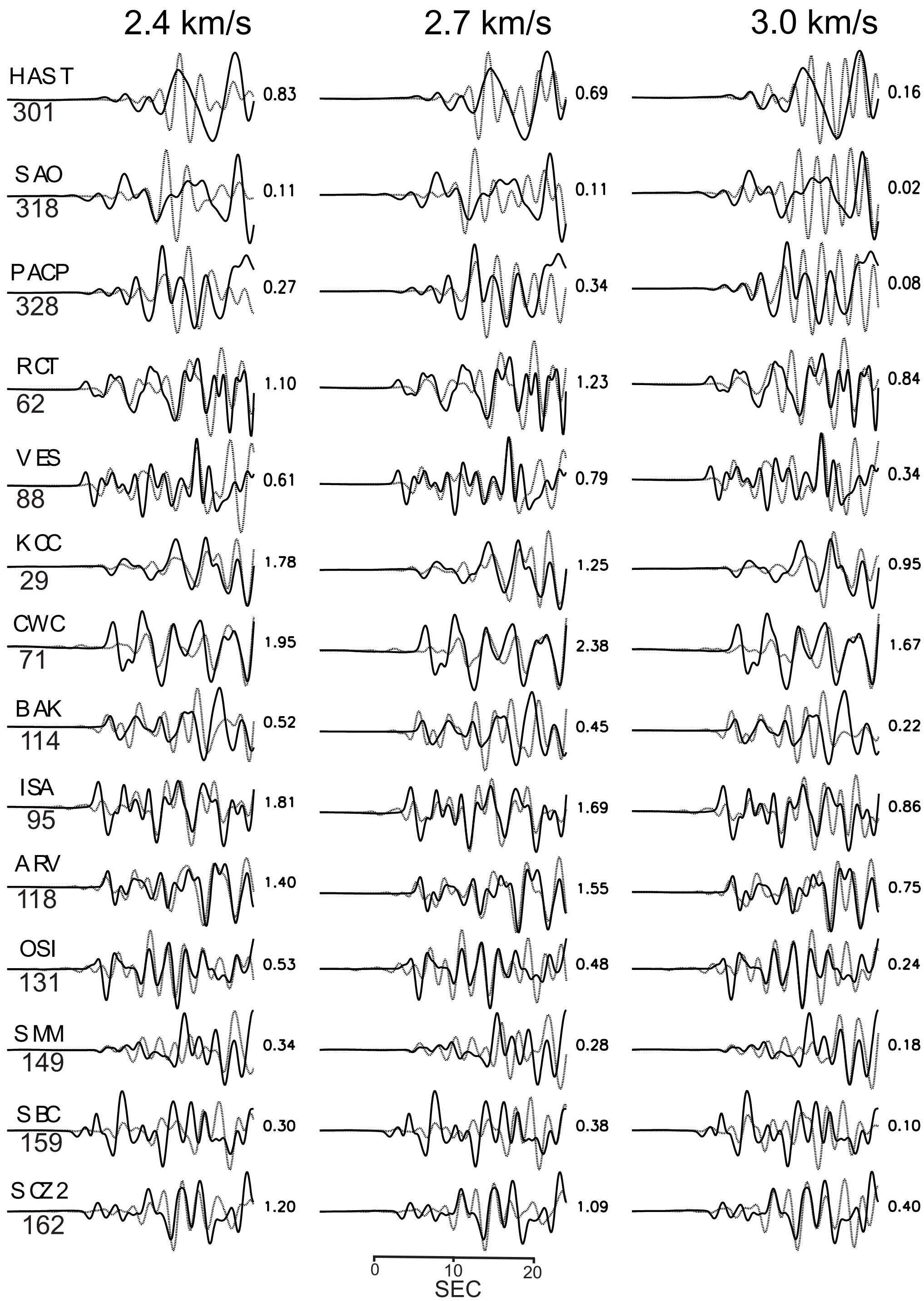

Figure 2. Fits between observed (solid line) and predicted (dashed line) vertical P_{nl} displacement waveforms for source models obtained using constant rupture velocities of 2.4, 2.7, and 3.0 km/sec. Numbers below the station names correspond to the azimuth in degrees from Table 1. Numbers to the right of each record pair indicate the ratio of synthetic-to-observed peak amplitudes for a seismic moment of 1.26×10^{25} dyne cm. Records are band-pass filtered between 0.1 and 0.5 Hz.

following the procedure described by Hartzell (1989). We used a 40×12 km fault subdivided into 120 2×2 km subfaults. A passband filter of 0.1–0.5 Hz was applied to both data and subfault responses prior to performing the inversion.

The EGF approach assumes that the aftershock record incorporates propagation effects along the travel path. However, because of limited suitable aftershocks, we do not consider variations of the EGF with depth and, as a result, assume similar waveforms for point sources downdip along

Table 3
Inversion Results for Different Crustal Structures and Rupture Velocities (V_R)

Crustal Model	V_R	$\|\mathbf{b} - \mathbf{Ax}\|$
NC	2.4	17.99
NC	2.7	17.86
NC	3.0	18.89
NF	3.0	18.39

$\|\mathbf{b} - \mathbf{Ax}\|$ is the Euclidean Norm of the residuals and measures the misfit between observed and synthetic records.

the fault. The results of the inversion indicate that this assumption does not pose a serious limitation for this source. The waveform fits (Fig. 5) are excellent for both vertical and horizontal records, which were included in the inversion due to the observed ability of the inversion process to predict all three components consistently. The fit between observed and predicted waveforms is remarkable considering the difficulties that we encountered using synthetic Green's functions.

In the EGF inversion, the spatial-smoothing and moment-minimization constraints are iteratively applied until the simplest solution is identified; we do not require that the total seismic moment correspond to a specific value. The resulting slip model (Fig. 6) yields a seismic moment of 1.57×10^{25} dyne cm, which is within the range of moment values previously estimated for the Parkfield earthquake. The distribution of coseismic slip shows a localized high-slip source (55 cm peak) near the hypocenter and a larger patch of slip (50 cm peak) between 6 and 20 km northwest of the hypocenter. This rupture pattern is consistent with detailed models of the coseismic slip inferred using both local strong-motion records (e.g., Custodio *et al.*, 2005; Liu *et al.*, 2006; Hartzell *et al.*, 2007) and geodetic data (e.g., Johanson *et al.*,

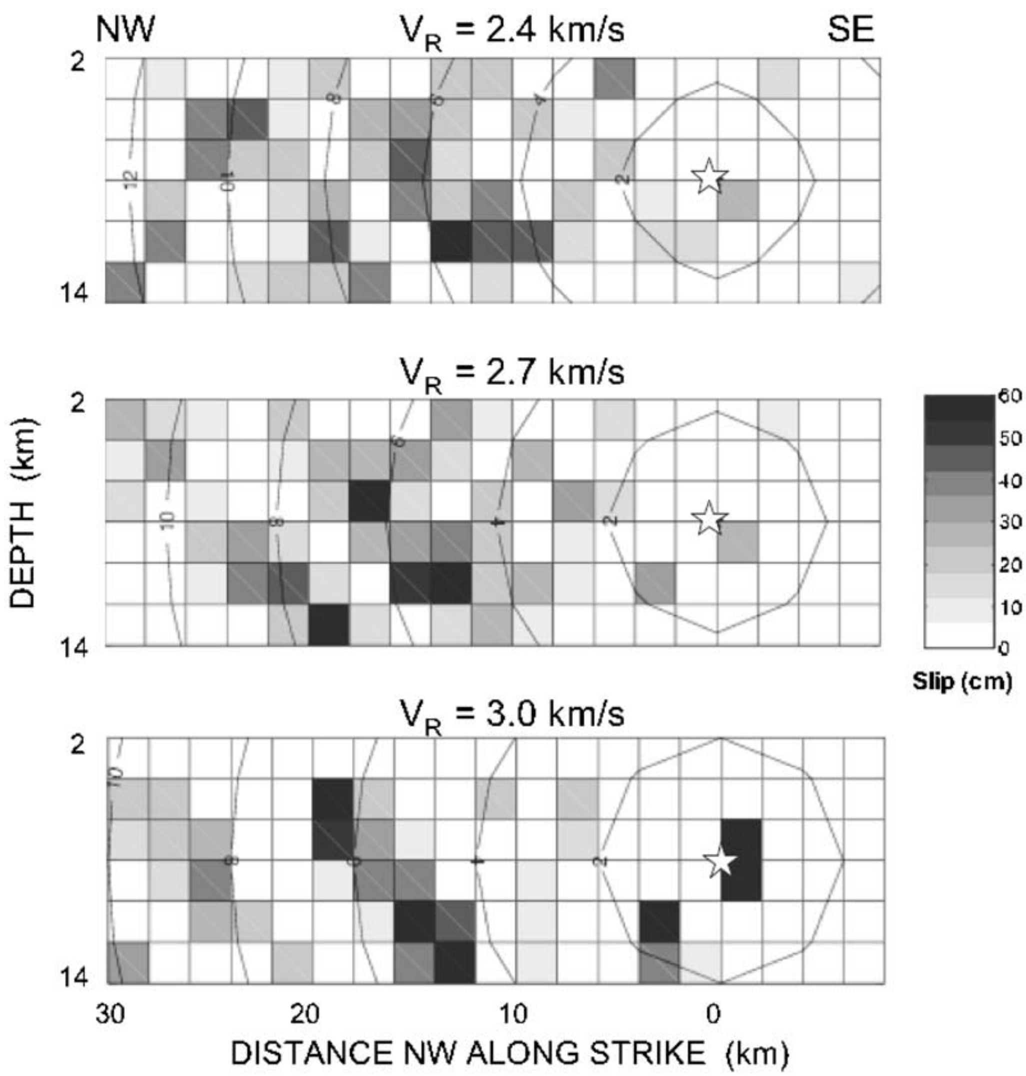

Figure 3. Coseismic slip models derived for the 2004 Parkfield earthquake using the default NC crustal structure from Table 2 and rupture velocities of 2.4 km/sec (top), 2.7 km/sec (middle), and 3.0 km/sec (bottom). The fault is subdivided into 114 2 × 2 km subfaults. The hypocenter (star) is at a depth of 8 km. Rupture time is contoured at 2 sec intervals along the fault.

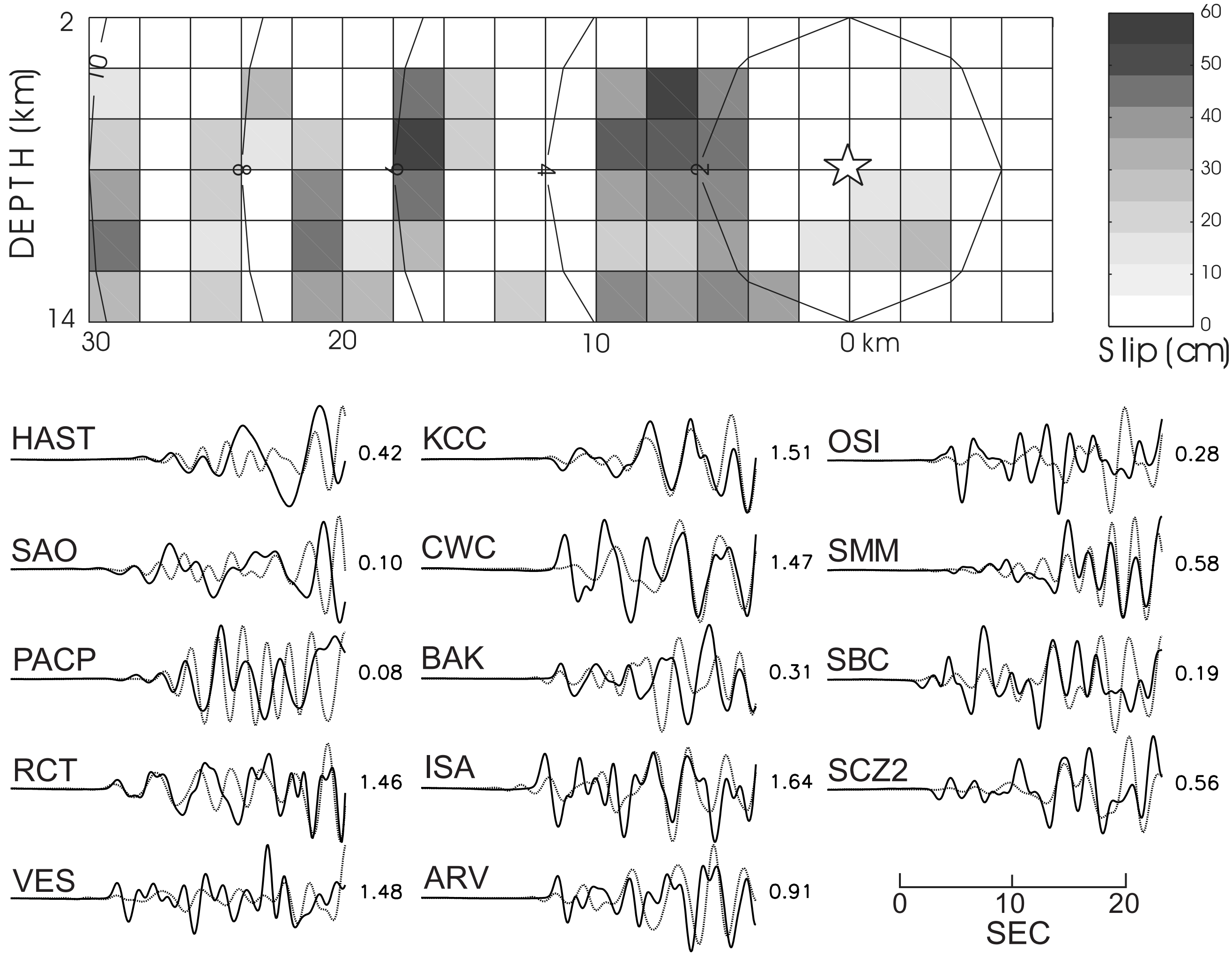

Figure 4. Inversion results obtained for the 2004 Parkfield earthquake using the NF crustal-velocity model from Table 2 assuming a constant rupture velocity of 3.0 km/sec. The coseismic slip model (top) is based on the same fault parameterization given in Figure 3. The bottom frame shows a comparison between the observed (solid line) and predicted (dashed line) band-pass-filtered vertical P_{nl} records. The ratio of synthetic-to-observed peak amplitudes for a seismic moment of 1.26×10^{25} dyne cm is shown for each record pair.

2006; Langbein *et al.*, 2006; Murray and Langbein, 2006), which show slip confined to two principal regions along the fault.

Conclusions and Discussion

We have applied a kinematic finite-fault inversion scheme to the P_{nl} displacement waveforms recorded within 2° of the 2004 Parkfield earthquake to recover the distribution of coseismic slip using both numerically calculated SGFs based on flat-layered 1D velocity models and EGFs derived from waveforms recorded for an M_w 5.0 aftershock. For the SGFs, fault slip is modeled using the default NCSN crustal structure for rupture velocities of 2.4, 2.7, and 3.0 km/sec. The inversion results indicate that a single constant rupture velocity cannot be uniquely identified based on the waveform fits. The corresponding slip models show slip expanding to the northwest with increasing rupture velocity to accommodate an earthquake rupture time of about 10 sec, indicating a weak dependence of the inversion results on the assumed rupture velocity. We also conducted the inversion using a more detailed velocity model based on the crustal structure northeast of the San Andreas Fault near Parkfield and found little evidence to indicate that this velocity structure is more representative of the different propagation paths. The corresponding source model has northwest slip located much closer to the hypocenter compared to the slip model derived using the default NCSN crustal velocities, indicating that reasonable variations in the assumed crustal model can affect the location of slip contributions along the fault.

Source models inferred using SGFs generally show some slip near the hypocenter and a larger separate patch of slip extending northwest along the fault. This slip pattern is consistent with source models previously obtained for the 2004 Parkfield earthquake using different data types and methodologies (e.g., Custodio *et al.*, 2005; Langbein *et al.*,

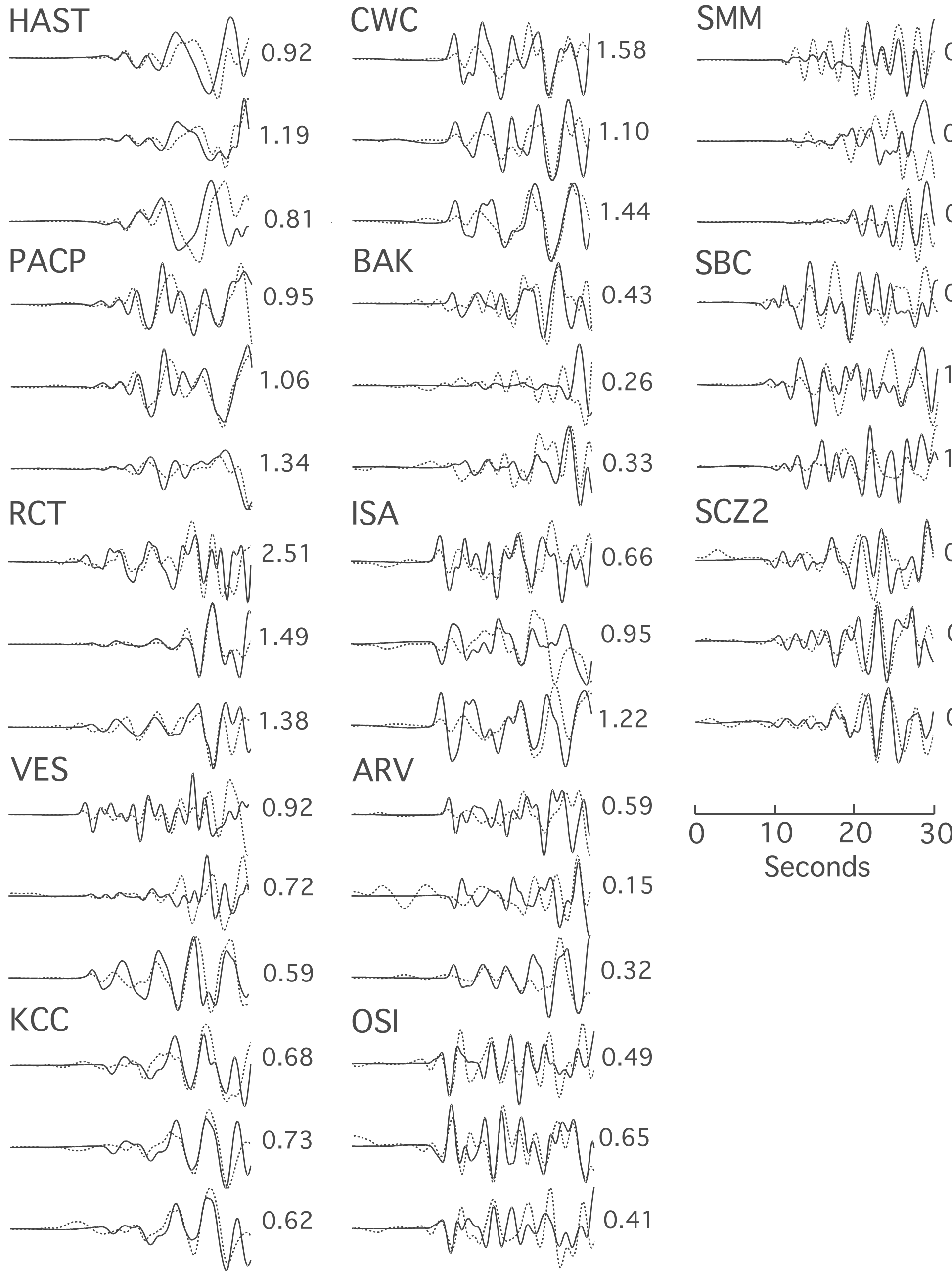

Figure 5. Comparison of observed (solid line) and predicted (dashed line) three-component P_{nl} waveforms for the coseismic slip distribution derived for the 2004 Parkfield earthquake using EGFs. Records for each station are shown in order for vertical, north–south, and east–west components. Waveforms are band-pass filtered between 0.1 and 0.5 Hz. Numbers to the right indicate the ratio of synthetic-to-observed peak amplitudes for an inferred seismic moment of 1.57×10^{25} dyne cm.

2005; Johanson *et al.*, 2006; Langbein *et al.*, 2006; Liu *et al.*, 2006; Murray and Langbein, 2006; Hartzell *et al.*, 2007), suggesting that SGFs can be used to derive a general first-order estimate of the coseismic distribution of slip using vertical P_{nl} waveforms. The P_{nl} records, however, cannot be fully reproduced along their entire length in the frequency range of 0.1 to 0.5 Hz. This general misfit is attributed to the inability of the assumed 1D crustal models to accurately represent the travel path to the different regional stations.

To minimize the effects of an inaccurate travel path, we conducted an inversion using EGFs based on waveforms recorded for an M_w 5.0 aftershock that occurred about 25 km northwest of the mainshock epicenter. The inversion results show a remarkable fit between observed and predicted waveforms for both vertical and horizontal records, indicating that the empirical procedure provides a powerful tool for the finite-fault analysis of regional waveforms. The inferred slip model is composed of two main regions of slip: a small lo-

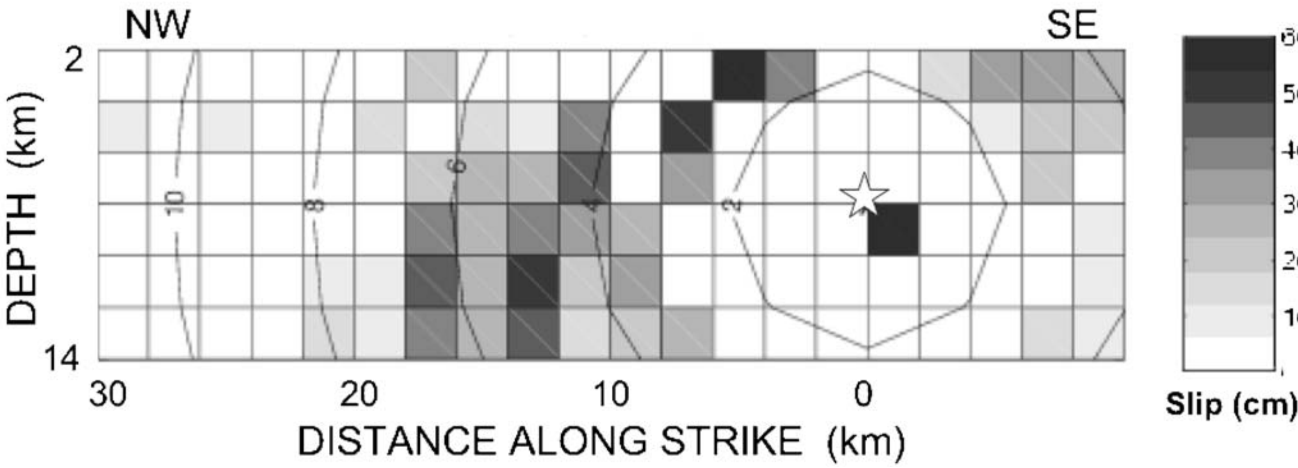

Figure 6. Coseismic slip model obtained for the 2004 Parkfield earthquake using EGFs and a rupture velocity of 3.0 km/sec. The fault is subdivided into 120 2×2 km subfaults. The hypocenter (star) is at a depth of 8 km. Rupture time is contoured at 2 sec intervals along the fault.

calized source near the hypocenter with a peak slip of 55 cm and a larger source (peak slip of about 50 cm) located between 6 and 20 km northwest of the hypocenter. In this approach, a single aftershock is used to identify Green's functions along the length and width of the fault plane. This differs from the traditional empirical approach used in modeling local strong-motion data (e.g., Hartzell, 1989), which uses multiple aftershocks to properly quantify the response for different depths. The single-aftershock method employed here, however, appears to do a reasonable job of constraining the slip model for the Parkfield earthquake using the regional P_{nl} recordings.

The results of this study also have implications for the routine application of finite-fault inversion schemes to regional seismic data using SGFs. In our analysis, we assumed a single coherent rupture pulse propagating at a constant speed across the fault. This assumption can significantly reduce the time required for the computation of coseismic slip patterns, for example, when using real-time data. In that case, a rise time appropriate for the earthquake, for example, estimated from the Somerville *et al.* (1999) relation between slip duration and seismic moment, can be used in the inversion. For the Parkfield earthquake, for example, the Somerville *et al.* (1999) relation yields an estimated rise time of 0.47 sec. Also, we required a solution whose seismic moment corresponds to the computed magnitude of the earthquake. This requirement was achieved by manually adjusting the amount of moment minimization but could be readily incorporated into the inversion scheme by appending a linear constraint that fixes the moment of the earthquake to a predetermined value. Such an approach has been previously suggested by Mendoza (1996) in the modeling of teleseismic data and avoids the iterative identification of both spatial-smoothing and minimization constraints required to stabilize the inversion problem. Thus, P_{nl} data may be useful for deriving a rapid estimate of the coseismic slip pattern for large earthquakes, although this would require the development of an automated algorithm that could be used in routine analysis.

Data and Resources

Seismic waveforms used in this study were obtained from the IRIS Data Management Center at www.iris.edu/data (last accessed July 2008) and were processed using the SAC2000 seismic analysis utility (Goldstein *et al.*, 2003). Earthquake locations were obtained from the Northern California Earthquake Data Center at www.ncedc.org (last accessed July 2008). Map plots were made with Generic Mapping Tools version 3.4.4 (Wessel and Smith, 1998).

Acknowledgments

This work was supported by the Consejo Nacional de Ciencia y Tecnologia (Project 46610) and by the U.S. Geological Survey. We thank G. Choy and W. Stephenson for internal reviews of the original manuscript. Comments by M. Mai and an anonymous reviewer also greatly improved the study.

References

Bakun, W. H., and A. G. Lindh (1985). The Parkfield, California earthquake prediction experiment, *Science* **229,** 619–624.

Bakun, W. H., B. Aagaard, B. Dost, W. L. Ellsworth, J. L. Hardebeck, R. A. Harris, C. Ji, M. J. S. Johnston, J. Langbein, J. J. Lienkaemper, A. J. Michael, J. R. Murray, R. M. Nadeau, P. A. Reasenberg, M. S. Reichle, E. A. Roeloffs, A. Shakal, R. W. Simpson, and F. Waldhauser (2005). Implications for prediction and hazard assessment from the 2004 Parkfield earthquake, *Nature* **437,** no. 13, 969–974, doi 10.1038/nature04067.

Custodio, S., P. Liu, and R. J. Archuleta (2005). The 2004 M_w 6.0 Parkfield, California, earthquake: inversion of near-source ground motion using multiple data sets, *Geophys. Res. Lett.* **32,** L23312, doi 10.1029/2005GL024417.

Goldstein, P., D. Dodge, M. Firpo, and L. Minner (2003). SAC2000: signal processing and analysis tools for seismologists and engineers, invited contribution to *The IASPEI International Handbook of Earthquake* *and Engineering Seismology*, W. H. K. Lee, H. Kanamori, P. C. Jennings and C. Kisslinger (Editors), Academic Press, London.

Hartzell, S. (1989). Comparison of seismic waveform inversion results for the rupture history of a finite fault: application to the 1986 North Palm Springs, California, earthquake, *J. Geophys. Res.* **94,** 7515–7534.

Hartzell, S. H., and T. H. Heaton (1983). Inversion of strong ground motion and teleseismic waveform data for the fault rupture history of the 1979 Imperial Valley, California, earthquake, *Bull. Seismol. Soc. Am.* **73,** 1553–1583.

Hartzell, S., P. Liu, C. Mendoza, C. Ji, and K. M. Larson (2007). Stability and uncertainty of finite-fault slip inversions: application to the 2004 Parkfield, California, earthquake, *Bull. Seismol. Soc. Am.* **97,** 1911–1934, doi 10.1785/0120070080.

Helmberger, D. V., and G. R. Engen (1980). Modeling the long-period body waves from shallow earthquakes at regional ranges, *Bull. Seismol. Soc. Am.* **70,** 1699–1714.

Jeffreys, H., and K. E. Bullen (1940). *Seismological Tables*, British Association for the Advancement of Science, Gray Milne Trust, London.

Johanson, I. A., E. J. Fielding, F. Rolandone, and R. Burgmann (2006). Coseismic and postseismic slip of the 2004 Parkfield earthquake from space-geodetic data, *Bull. Seismol. Soc. Am.* **96,** S269–S282, doi 10.1785/0120050818.

Kaverina, A., D. Dreger, and E. Price (2002). The combined inversion of seismic and geodetic data for the source process of the 16 October 1999 M_{w} 7.1 Hector Mine, California, earthquake, *Bull. Seismol. Soc. Am.* **92,** 1266–1280.

Langbein, J., J. R. Murray, and H. A. Snyder (2006). Coseismic and initial postseismic deformation from the 2004 Parkfield, California, earthquake observed by Global Postioning System, electronic distance meter, creepmeters, and borehole strainmeters, *Bull. Seismol. Soc. Am.* **96,** S304–S320, doi 10.1785/0120050823.

Langbein, J., R. Borcherdt, D. Dreger, J. Fletcher, J. L. Hardebeck, M. Hellweg, C. Ji, M. Johnston, J. R. Murray, R. Nadeau, M. J. Rymer, and J. A. Treiman (2005). Preliminary report on the 28 September 2004 *M* 6.0 Parkfield, California, earthquake, *Seism. Res. Lett.* **76,** 10–26.

Liu, P., S. Custodio, and R. J. Archuleta (2006). Kinematic inversion of the 2004 *M* 6.0 Parkfield earthquake including an approximation to site effects, *Bull. Seismol. Soc. Am.* **96,** S143–S148, doi 10.1785/0120050826.

Mendoza, C. (1996). Rapid derivation of rupture history for large earthquakes, *Seism. Res. Lett.* **67,** 19–26.

Murray, J., and J. Langbein (2006). Slip on the San Andreas Fault at Parkfield, California, over two earthquake cycles and the implications for seismic hazard, *Bull. Seismol. Soc. Am.* **96,** S288–S303, doi 10.1785/0120050820.

Oppenheimer, D., F. Klein, J. Eaton, and F. Lester (1993). The Northern California Seismic Network bulletin, January–December 1992, *U.S. Geol. Surv. Open-File Rept. 93-578*, 18 pp.

Roeloffs, E., and J. Langbein (1994). The earthquake prediction experiment at Parkfield, California, *Rev. Geophys.* **32,** 315–336.

Somerville, P., K. Irikura, R. Graves, S. Sawada, D. Wald, N. Abrahamson, Y. Iwasaki, T. Kagawa, N. Smith, and A. Kowada (1999). Characterizing crustal earthquake slip models for the prediction of strong ground motion, *Seism. Res. Lett.* **70,** 59–80.

Thurber, C., H. Zhang, F. Waldhauser, J. Hardebeck, A. Michael, and D. Eberhart-Phillips (2006). Three-dimensional compressional wavespeed model, earthquake relocations, and focal mechanisms for the Parkfield, California, region, *Bull. Seismol. Soc. Am.* **96,** S38–S49, doi 10.1785/0120050825.

Wallace, T. C., D. V. Helmberger, and G. R. Mellman (1981). A technique for the inversion of regional data in source parameter studies, *J. Geophys. Res.* **86,** 1679–1685.

Wessel, P., and W. H. F. Smith (1998). New improved version of the Generic Mapping Tools released, *Eos Trans. AGU* **79,** 579.

Zhu, L., and L. A. Rivera (2002). A note on the dynamic and static displacements from a point source in multilayered media, *Geophys. J. Int.* **148,** 619–627.

Centro de Geociencias
Universidad Nacional Autonoma de Mexico
Campus Juriquilla
Queretaro, Mexico
(C.M.)

U.S. Geological Survey
Box 25046
MS 966
Denver Federal Center
Denver, Colorado
(S.H.)

Manuscript received 21 November 2007